

Chapter 2

Theory of Organic Semiconductor Lasers

2.1 Introduction

The acronym laser stands for ‘light amplification by stimulated emission of radiation’. As early as 1960, Maiman demonstrated the first laser using a ruby crystal as the active medium, pumped by a flash lamp [1]. Later in 1962, the first semiconductor laser was demonstrated by two groups led by Robert Hall [2] and Marshall Nathan [3], respectively. The first visible wavelength laser diode was reported later in that same year by Holonyak [4]. These semiconductor lasers could only operate with pulsed currents and at liquid nitrogen temperature (77 K). In 1969, room-temperature, continuous-operation diode lasers using heterojunction structures were demonstrated by a team including Dmitri Garbuzov and Zhores Alferov [5] (winner of the 2000 Nobel Prize for Physics) and by the competing team of Izuyo Hayashi and Morton Panish [6]. The year 2012 marks the 50th anniversary of the invention of first semiconductor laser. During these last 50 years, semiconductor lasers have experienced remarkable development; products are now ubiquitous, covering from pure science research including spectroscopy and bio-sensing, to our daily lives such as CD/DVD players, optical mice, laser pointers and so on.

Organic semiconductor lasers (OSLs), on the other hand, are a relatively new member of the laser family. The first laser using a conjugated polymer as the gain medium was reported in 1992 by Moses [7]. In 1996, Tessler and co-workers demonstrated the first optically pumped organic microcavity laser [8]. Available OSLs nowadays are optically pumped by additional light sources such as inorganic solid-state lasers or inorganic deep-blue laser diodes, and recently light emitting diodes. With a diverse range of resonators and substrates, organic lasers offer outstanding tunability, low-cost production and mechanical flexibility.

This chapter gives an introduction to the fundamentals of organic semiconductors and lasers. In [Sect. 2.2](#), the origins of semi-conductivity in conjugated molecules is discussed and the basic electrical and optical concepts for organic semiconductors are described. The types of commonly used organic semiconductors for lasers are listed in [Sect. 2.3](#). The optical properties of organic

semiconductors including absorption, fluorescence, gain and loss are described in Sect. 2.4. Section 2.5 discusses various resonators and pump sources for organic lasers as well as the output beams from these plastic lasers.

2.2 Electronic Properties

2.2.1 Conjugated Molecules

The essential element for an organic molecule is carbon (C). It is the building block of many types of polymers by forming long chains of interconnecting C–C bonds. Each atom of carbon consists of six electrons which occupy in different orbitals around the central nucleus. For a ground-state carbon atom, the electron configuration of $1s^2 2s^2 2p^2$ is shown in Fig. 2.1a. The two electrons in the 1s orbital are considered to be core electrons and are not available for bonding. There are four remaining valence electrons, two paired in the 2s orbital, and two unpaired in the 2p orbital which are able to form two bonds. The spatial distribution of the s and p orbitals are shown in Fig. 2.2 [9].

As energy is released when bonds form, carbon tries to maximize the number of bonds it can form. For this reason, an excited state carbon is formed by promoting one of its 2s electrons into its empty 2p orbital resulting in four unpaired electrons, which are able to form four bonds, see Fig. 2.1b. The excited state configuration is therefore $1s^2 2s^1 2p^3$. This process is favourable because of the arrangement of electrons leading to less repulsion and hence more stability.

In organic molecules, the atomic orbitals in carbon can hybridize into different geometries. The exact orbital hybridization is dependent on the bonding of the atoms. For example for a carbon atom in a methane (CH_4) molecule, sp^3 hybridization is produced. The filled 2s combines with two half filled 2p orbitals to become four half filled sp^3 hybridized orbitals. The model in Fig. 2.3a illustrates the bonding in methane. In the methane molecule, the carbon's four sp^3 hybridized orbitals point to the corners of hydrogen. The hydrogen orbitals overlap with them to form four C–H bonds which are 109.5° apart, equally spread in 3D with carbon at the centre of the tetrahedron grouping of single bonded atoms.

Fig. 2.1 Electron configuration of **a** ground state (lowest energy state) and **b** excited state carbon

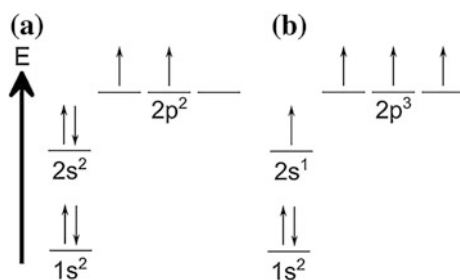


Fig. 2.2 Spatial distribution of **a** 2s and **b–d** three 2p orbital clouds

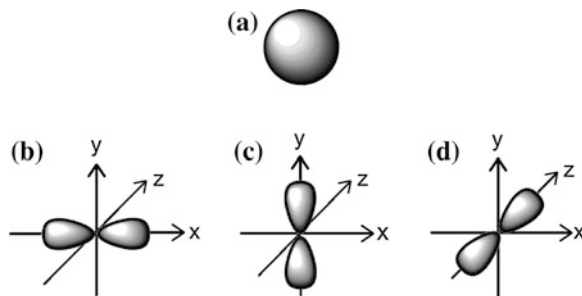
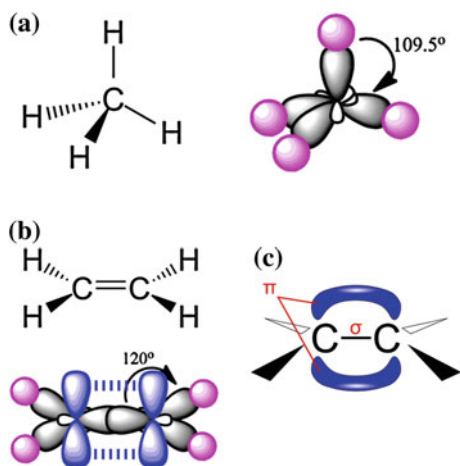


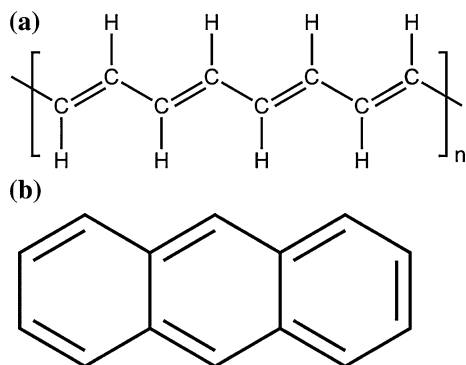
Fig. 2.3 Molecular bonding in **a** methane and **b** ethylene; **c** a C = C double bond includes both σ and π bonds



The bonding is different in trigonal planar groupings which include a C = C double bond. Considering the double bond in ethylene ($\text{CH}_2 = \text{CH}_2$), the 2s orbital and two half filled 2p orbitals mix to become three half filled sp^2 hybridized orbitals, and the fourth electron occupies an unhybridized 2p. The unhybridized 2p is perpendicular to the trigonal plane of three sp^2 hybrids which are axially symmetric and 120° apart from each other, presented in Fig. 2.3b. The two sp^2 orbitals facing each other overlap to form a σ bond, and the overlapping between the two parallel 2p orbitals is the origin of the formation of a π bond, as shown in Fig. 2.3c. In an ethylene molecule, there are four hydrogen atoms which overlap with the rest of the four sp^2 orbitals.

A backbone of conjugated polymer molecules consists of alternating single and double carbon bonds, forming a long-chain molecule, sometimes containing benzene rings. The σ bond is responsible for the rigidity of the C = C bond. More importantly, compared to the σ bond, the π bond is weak resulting in electron delocalisation along the backbone of the molecule. In other words, instead of being localised to an orbital associated with a specific bond, the π orbitals spread above and below the atoms and allow the electrons to move from one carbon to another

Fig. 2.4. Chemical structure of **a** polyacetylene and **b** anthracene, consisting of alternating double and single carbon bonds



along the entire backbone. Therefore directional conductivity can be produced along the axis of the so-called conjugated polymer chain. Figure 2.4 represents two typical semiconducting molecules, polyacetylene and anthracene. In an anthracene molecule, the π bond orbitals actually join up to form a ring-shaped orbital above and below the plane of each benzene ring. When three benzene rings are fused together it ends with a continuous π bond orbital region enabling conductivity, as shown in Fig. 2.5 [9].

2.2.2 Energy Levels

When two carbon atoms approach each other and form a molecular bond, it is also possible that their p-orbital electrons interfere destructively, i.e. out of phase, to

Fig. 2.5 **a** Six p-orbitals in the benzene ring; **b** these six orbitals interact with each other freely and become delocalized; **c** the π bond orbital from each ring join up in anthracene, resulting in a continuous π orbital locating above and below the molecule. The π orbitals below the molecule are not shown in this figure

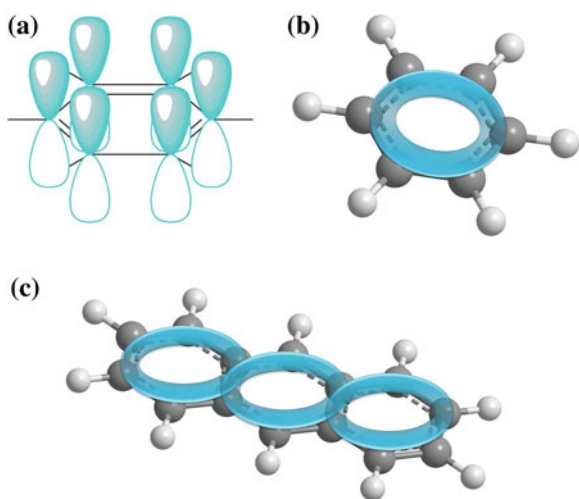
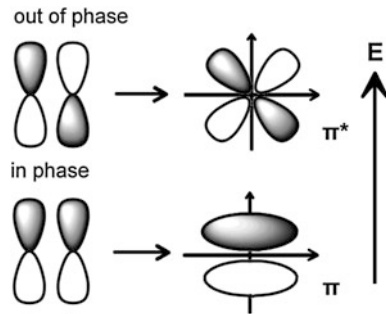


Fig. 2.6 π and π^* orbitals

form an antibonding orbital π^* , see Fig. 2.6. When the π^* orbitals are occupied, the energy of the molecule is higher than when the π orbital is occupied. The difference in the energy of π – π^* orbitals forms an energy gap. The highest energy π orbital is occupied by two electrons at thermal equilibrium and is referred to as the HOMO (highest occupied molecular orbital). The lowest unoccupied antibonding π^* orbital is referred to as the LUMO (lowest unoccupied molecular orbital). The energy difference between the HOMO and LUMO is termed the HOMO–LUMO gap, i.e. energy gap. An electron can move from the π to the π^* molecular orbital when there is appropriate excitation, forming an exciton (a bound electron–hole pair). Relaxation occurs with the electron moving back down to the π orbital.

Since two electrons can occupy each π or π^* energy level, the spin of electrons need to be considered. There are four possible spin combinations at each energy level, such as

$$\uparrow\uparrow, \uparrow\downarrow, \downarrow\uparrow, \downarrow\downarrow \quad (2.1)$$

The singlet state is anti-symmetric hence the total spin angular momentum $s = 0$, while for the triplet state, $s = 1$.

$$|0, 0\rangle = \frac{1}{\sqrt{2}}(\uparrow\downarrow - \downarrow\uparrow) \Rightarrow s = 0 \text{ (Singlet)} \quad (2.2)$$

$$\left. \begin{aligned} |1, 1\rangle &= \uparrow\uparrow \\ |0, 0\rangle &= \frac{1}{\sqrt{2}}(\uparrow\downarrow + \downarrow\uparrow) \\ |1, -1\rangle &= \downarrow\downarrow \end{aligned} \right\} \Rightarrow s = 1 \text{ (Triplet)} \quad (2.3)$$

The electron transition in singlet or triplet states is restricted by spin-selection rules [10]. Transitions are only allowed between same-spin states, i.e. singlet to singlet or triplet to triplet, whereas singlet–triplet transitions are forbidden.

2.3 Types of Organic Semiconductors

Organic semiconductors can be categorised into several groups based on their chemical structures and how they are processed. Early studies were focused on single crystals of organic molecules. A typical example is anthracene [8]; its molecular structure is shown in Fig. 2.4b, however, extremely high voltages were needed for it to emit light. The difficulty in the growing and handling of these crystals made other types of materials more attractive for light emission. Evaporation of small-molecule organic-semiconductors in order to deposit thin films that provide efficient electroluminescence attracted serious interest from the late 1980s. Aluminum tris(quinolate) (Alq_3), shown in Fig. 2.7a, is an example of small molecule organic semiconductors.

Another important member of the organic family is conjugated polymers. Development of polymerisation techniques allowed the synthesis of conjugated polymers which have long backbones of carbon, mentioned in Sect. 2.2. The most commonly used conjugated polymers as laser materials are the poly(phenylene

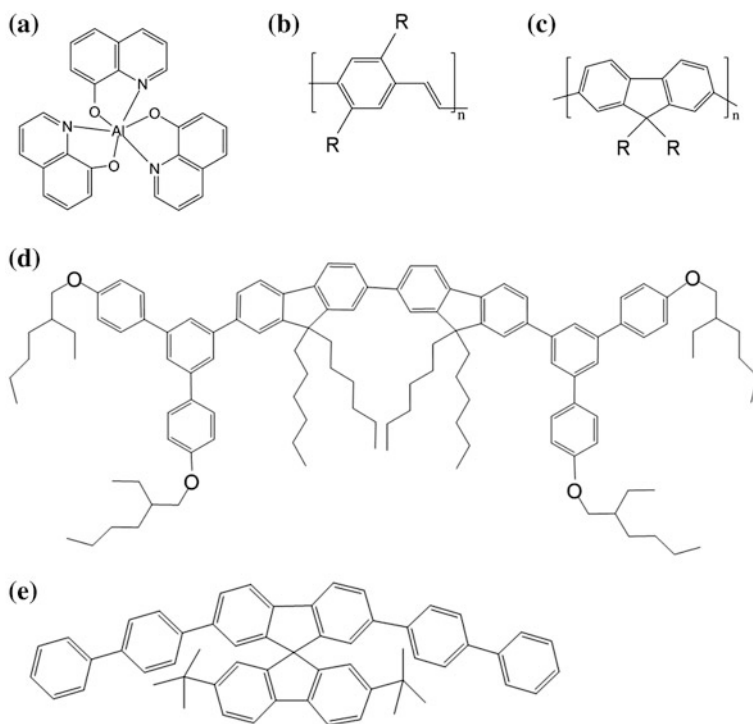


Fig. 2.7 Chemical structures of typical organic semiconductors used for lasers: **a** aluminum tris(quinolate); **b** generic poly(para-phenylene vinylene) derivative; **c** generic polyfluorene derivative; **d** bisfluorene cored dendrimer; **e** spiro-linked oligomer

vinylene) (PPV) [9, 11, 12] and the polyfluorene (PF) derivatives [13], shown in Fig. 2.7b, c respectively. A major difference from the small molecule organic semiconductors is that conjugated polymers are solution processible, which significantly simplifies the fabrication of the light-emitting devices such as lasers and light-emitting diodes. The materials discussed in Chaps. 5, 6 and 8 belong to this category.

Two further categories of organic semiconductors are conjugated dendrimers [14, 15] and oligomers [16, 17]. A conjugated dendrimer typically consists of a chromophore core defining the photophysical properties of the molecule, several conjugated dendrons (branches) controlling the intermolecular interactions of the emissive cores, and surface groups attached to their ends providing solubility. Figure 2.7d shows an example of these highly branched architectures. This is a first generation dendrimer - one level of branching with a bisfluorene core [18]. In contrast to polymers, the final category, oligomers, have a limited and known number of repeating monomer units. These materials have remarkable performance in light emitting devices [19]. Figure 2.7e shows an example of a successful lasing material, with two oligomers linked by a spiro linkage [16]. The star-shaped molecules to be discussed in Chap. 4 also belong to this category.

2.4 Optical Properties

2.4.1 Absorption and Emission of Light

As mentioned in Sect.2.2.2, the electronic transitions between π and π^* orbitals are responsible for the absorption and emission of photons. The energy of the absorbed photon equals the energy gap between π and π^* states. As the conjugation length increases, the HOMO–LUMO gap decreases, hence the energy required for the electronic transitions becomes lower, i.e. the absorption wavelength gets longer, see Table 2.1.


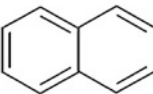
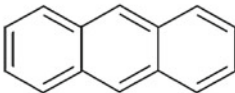
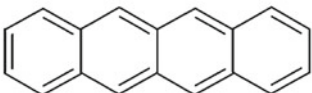
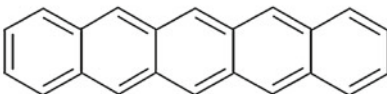
The interaction strength of the light with the material is expressed by the Beer Lambert Law equation:

$$I = I_0 \exp(-\alpha z) \quad (2.4)$$

where α is the absorption coefficient, z is the light path length in the material, I is the intensity of light out and I_0 is the intensity of the incident light.

The emission of light in conjugated molecules can be explained with the aid of the Franck–Condon principle [21]. As shown in Fig. 2.8, S_0 and S_1 represent the ground and first excited singlet states respectively, which split into a series of vibronic states from the lowest energy level, numbered 0 upwards. In a simplified situation, absorption occurs when an incoming photon excites an electron from the lowest electronic ground state S_0 to an unpopulated higher singlet state S_1 , followed by a fast, non-radiative relaxation to the 0th vibronic level in S_1 . A radiative decay process occurs from the 0th vibronic level in S_1 back to the ground state S_0 .

Table 2.1 The principal value of the absorption wavelength as increasing numbers of benzene rings [20]

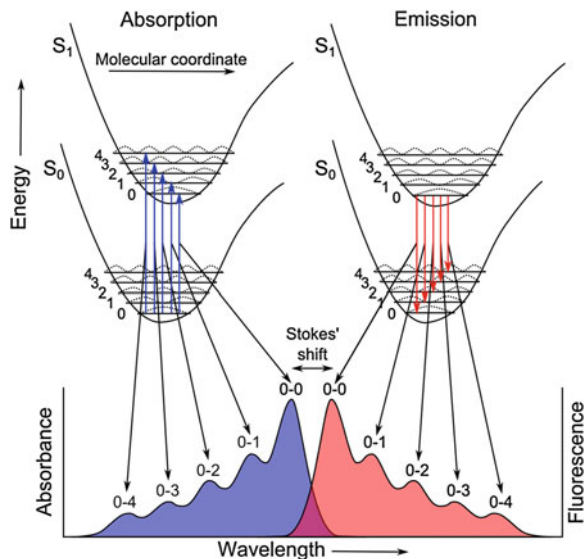
Molecule	Structure	Absorption peak (nm)
Benzene		255 nm
Napthalene		315 nm
Anthracene		380 nm
Tetracene		480 nm
Pentacene		580 nm

and again, rapidly relaxes non-radiatively to the bottom of the ground state, 0th vibronic level in S_0 . In conjugated molecules, the separation between the absorption and fluorescence spectrum, known as the Stokes' shift, is due to the energy loss between where a photon is absorbed and where it is emitted [22]. One common loss mechanism is the interaction between the electrons and the carbon lattice, which results in an energy displacement between the ground state and excited state under the coordinate of the distance between neighbouring carbon atoms. The disordered environment in long-chain polymers, i.e. different conjugation lengths at different locations forming various localized energy states, also extends the Stokes' shift in conjugated molecules.

A large energy shift in organic semiconductor molecules will result in less self-absorption. It also helps to increase the photoluminescence quantum yield (PLQY), leading to lower lasing thresholds. Further reduction of the spectral overlap between absorption and fluorescence spectra can be achieved by polymer blending or by doping with dye molecules [23, 24].

Optical transitions in conjugated molecules are not single wavelength transitions, but broadened as presented in Fig. 2.8. This broadening is characterised as both homogeneous and inhomogeneous broadening [25]. This means that the absorption and emission throughout the conjugated molecules have a fluctuating

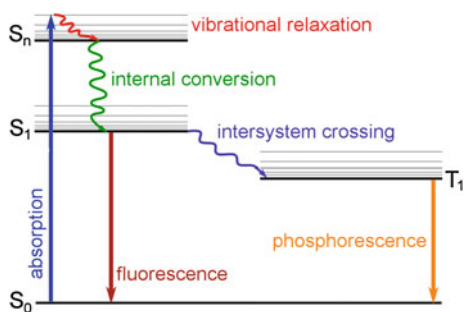
Fig. 2.8 Schematic representation of the absorption and emission spectrum with corresponding energy diagram



disorder which is the same for all the atoms, for example due to heat, and also a static disorder, for example due to conformation change such as broken conjugation in the long chains.

In a realistic situation, there are more complicated transition processes happening in a conjugated molecule, as illustrated in Fig. 2.9. When the photo-excited electron non-radiatively relaxes to the lower energy state in S_1 , it is possible for the population to migrate to the triplet manifold, T_1 , by intersystem crossing; however this requires a spin-flip of an electron between the singlet and triplet state. To return radiatively to the ground state, another spin-flip is required. This process produces phosphorescence, however, has a much lower probability, in other words, weaker intensity and longer radiative lifetime compared to fluorescence produced with the S_1 to S_0 transition. In most organic semiconductors, phosphorescence is a very inefficient process [26]. Efficient phosphorescence were only observed in organometallic materials [27, 28].

Fig. 2.9 A Jablonski diagram showing the various transition processes in a conjugated organic molecule (adapted from Ref. [20])



The efficiency of the fluorescence process is quantified by the PLQY, which is defined as the number of photons emitted divided by the number of photons absorbed [29]. With the presence of the non-radiative decay mechanisms, the PLQY of organic semiconductors is always below 100 %. The lifetime of an emissive molecule, i.e. the measured natural lifetime, τ_{PL} , is related to the radiative (k_{rad}) and non-radiative ($k_{non-rad}$) rate by Eq. (2.6):

$$\tau_{PL} = \frac{1}{k_{rad} + k_{non-rad}} \quad (2.5)$$

The fluorescence yield, Φ , is defined by the expression:

$$\Phi = \frac{k_{rad}}{k_{rad} + k_{non-rad}} \quad (2.6)$$

Thus the radiative lifetime, τ_{rad} is simply related to its natural lifetime and PLQY by:

$$\tau_{rad} = \frac{\tau_{PL}}{\Phi} \quad (2.7)$$

For triplet phosphorescence in conventional organic materials, k_{rad} is very small so that $k_{non-rad}$ dominates and the PLQY is very low.

2.4.2 Light Amplification in Organic Semiconductors

Two energy levels, E_1 and E_2 ($E_1 < E_2$), are illustrated in Fig. 2.10 to explain the phenomenon of spontaneous emission and stimulated emission. The frequency of the radiated wave is given by the well-known equation [30]:

$$\nu = \frac{E_2 - E_1}{h} \quad (2.8)$$

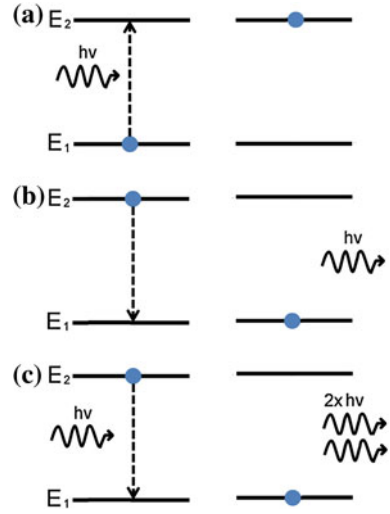
where h is Planck's constant. Spontaneous emission is characterized by the emission of a photon of energy of νh with random phase, whereas stimulated emission is induced by the incident wave and the emission from all molecules adds in phase to that of the incoming wave and in the same direction, i.e. they are coherent.

Stimulated absorption changes the upper state E_2 population, N_2 by:

$$\frac{dN_2}{dt} = B_{12}\rho_\nu N_1 \quad (2.9)$$

where B_{12} is the Einstein 'B' coefficient for the transition $E_1 \rightarrow E_2$, related to the absorption cross section, ρ is the photon density at frequency ν and N_1 is the population of the lower state E_1 . In the spontaneous emission process, the rate of decay of N_2 , is given by:

Fig. 2.10 Schematic illustration of **a** absorption, **b** spontaneous emission and **c** stimulated emission



$$\frac{dN_2}{dt} = -\frac{N_2}{\tau_2} \quad (2.10)$$

where τ_2 is the lifetime of the upper state. In the stimulated emission process, the rate of decay of N_2 , is given by:

$$\frac{dN_2}{dt} = -B_{21}\rho_\nu N_2 \quad (2.11)$$

For a system in thermal equilibrium, the ratio of the population in the two energy states is given by Boltzmann statistics:

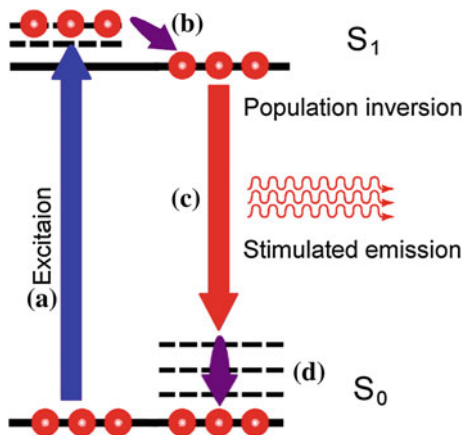
$$\frac{N_1}{N_2} = \frac{g_1}{g_2} \exp\left(\frac{E_2 - E_1}{kT}\right) = \frac{g_1}{g_2} \exp\left(\frac{h\nu}{kT}\right) \quad (2.12)$$

where g_1 and g_2 are the degeneracy of energy states E_1 and E_0 respectively, k is the Boltzmann's constant and T is the temperature in Kelvin.

According to Eq. (2.12), under equilibrium, $N_2 < g_2 N_1 / g_1$, which means the material always acts as an absorber. However, if a non-equilibrium condition is achieved, i.e. $N_2 > g_2 N_1 / g_1$, then the material acts as an amplifier. This condition is known as population inversion. The population inversion is the necessary condition for light amplification through a medium.

To obtain light amplification we use media with more than two energy states. As such all practical gain systems can be simplified to three or four energy levels; organic semiconductors are no exception. For a conjugated material, the energy level system resembles that of a four level laser. As the thermal relaxations are substantially faster (~ 10 ps) than the radiative decay (~ 1 ns), allowing a population inversion to be maintained relatively easily, as shown in Fig. 2.11.

Fig. 2.11 Energy levels of the lowest two singlet states in an organic semiconductor, including the corresponding optical and thermal transitions—**a** excitation from the ground state into excited state; **b** fast non-radiative relaxation; **c** stimulated emission from S_1 to S_0 ; **d** fast non-radiative decay to the lowest vibronic ground state



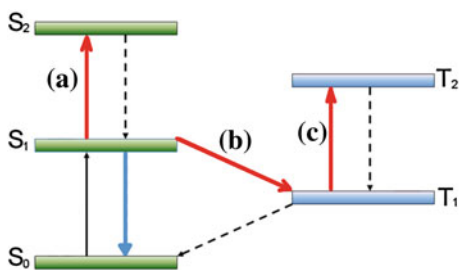
The gain coefficient is simply the product of the stimulated emission cross section, σ , and the population inversion, defined by:

$$g = \sigma(N_2 - N_1) \quad (2.13)$$

However, several mechanisms are present in organic semiconductors that can deplete the excited state population non-radiatively. One of the mechanisms is the presence of chemical defects and impurities in a conjugated polymer, resulting in efficient quenching of the singlet photoluminescence [31]. Another possible mechanism is exciton–exciton annihilation due to collisions of excitons travelling along the backbone of a conjugated polymer [11]. This occurs at relatively high excitation densities, leading to electron and hole polaron generation thus reducing the number of the excitons that could contribute to fluorescence [32].

Apart from the above depletion mechanisms, there are some other optical losses present in the organic semiconductor gain media, including the spectrum overlap induced self-absorption that mentioned in Sect. 2.4.1, singlet excited state absorption, intersystem crossing and even triplet–triplet excited state absorption [33, 34], as illustrated in Fig. 2.12. In reality in order to achieve light amplification, sufficient gain is required to overcome not only the stimulated absorption in the material but also the various losses. With all these losses taken into consideration, the net gain

Fig. 2.12 **a** Singlet excited state absorption; **b** intersystem crossing and **c** triplet excited state absorption



(gain minus loss) in organic semiconductors can still be very high. Net gains over 60 cm^{-1} have been measured in a wide range of organic materials [35].

2.5 Organic Semiconductor Lasers

Once a population inversion is established, the gain medium will amplify an incident beam of light. To operate as a laser, another two elements are required, a feedback resonator and an excitation source. The optical amplifier is responsible for the generation of photons via either an optical or electrical excitation, while the resonator acts as a feedback cavity that forces the photons to travel several times through the amplifier and thus cause laser oscillation.

2.5.1 Resonators for Organic Lasers

The simplest organic laser resonator is two parallel mirrors with a slab of gain material placed in between, to form a Fabry–Perot cavity as shown in Fig. 2.13a. The resonant wavelengths are determined by the condition:

$$\lambda = \frac{2nL}{m} \quad (2.14)$$

where n is the refractive index of the gain material inside the cavity, L is the cavity length and m is an integer. Organic semiconductor lasers (OSLs) with this type of resonator are easy to fabricate; the organic gain medium can be either in solution or in a solid-state film [7, 13]. Due to the high gain (and strong absorption) in organic semiconductors, the gain medium thickness is required to be only in the order of hundreds of nm to achieve lasing.

Other types of resonator configurations for OSLs, including micro-ring and micro-sphere cavities, are illustrated in Fig. 2.13b, c. These types of microcavity normally lead to a multi-longitudinal mode output, and the quality of the emitted beam is usually not good as the light is emitted in multiple directions.

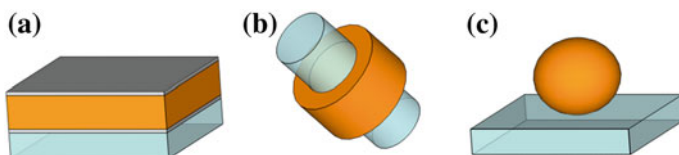


Fig. 2.13 Schematic resonators used in organic semiconductor lasers **a** Fabry–Perot microcavity; **b** micro-ring resonator, i.e. an optical fibre coated with polymer; **c** spherical microcavity

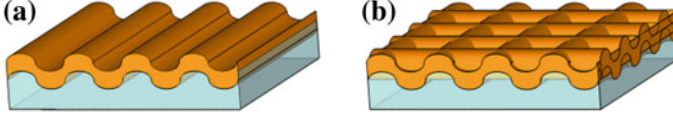


Fig. 2.14 Schematic illustration of **a** one-dimensional and **b** two-dimensional distributed feedback grating in glass coated with a layer of organic thin film

In the literature, low threshold organic semiconductor lasers have been demonstrated mainly with distributed feedback (DFB) resonators and distributed Bragg reflectors (DBR) [19, 36, 37]. In this section, I focus on the DFB cavities, which are frequently used in this thesis. Chapters 3–6 will discuss in detail the DFB cavity fabrication, their low threshold operation and the spectral tunability of emission. Figure 2.14 shows schematic of one-dimensional (1D) and two-dimensional (2D) DFB resonators.

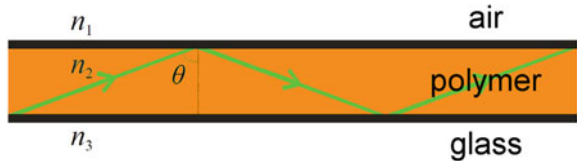
An organic DFB laser consists of a thin film and a corrugated substrate. Waveguide theory can be used to explain how the light is confined within the organic semiconductor film [38]. Here we first do not consider the corrugation in the substrate. A slab waveguide of organic semiconductor film is structured as Fig. 2.15, allowing light to travel long distances in the planar film without diverging, i.e. the optical ray follows a repetitive, zigzag path in the film.

Guiding is achieved by using a structure consisting of a high refractive index region surrounded by regions of lower refractive indices which are known as the cladding. In this case the organic film is the high index element ($n_2 > 1.46$), sandwiched by low index air ($n_1 = 1$) and glass substrate ($n_3 = 1.46$). The light is well confined in the polymer layer by total internal reflection. The effective refractive index, n_{eff} , is determined by the whole waveguide design. The equation for waveguide mode is given as [38]

$$\frac{4\pi d}{\lambda} \sqrt{n_p^2 - n_{eff}^2} = \Phi_a + \Phi_s + 2m\pi \quad (2.15)$$

where n_p is the refractive index of polymer, d is the polymer film thickness, λ is the light wavelength, m is an integer, ϕ_a and ϕ_s are the phase shift upon total internal reflection at the polymer/air and polymer/glass interface respectively. For the transverse electric (TE) mode, ϕ_a and ϕ_s can be obtained using

Fig. 2.15 Schematic illustration of a planar optical waveguide



$$\phi_b = 2 \tan^{-1} \left(\sqrt{\frac{n_{eff}^2 - n_b^2}{n_p^2 - n_{eff}^2}} \right); \quad b \equiv a, f \quad (2.16)$$

For the transverse magnetic (TM) mode, Φ_a and Φ_s can be obtained using

$$\phi_b = 2 \tan^{-1} \left(\frac{n_p^2}{n_b^2} \sqrt{\frac{n_{eff}^2 - n_b^2}{n_p^2 - n_{eff}^2}} \right); \quad b \equiv a, f \quad (2.17)$$

The allowed range for the effective refractive index of all guided modes is defined as

$$\text{Max}\{n_a, n_s\} \leq n_{eff} \leq n_p \quad (2.18)$$

For each propagation mode there is a critical film thickness, so called cut-off thickness for example d_0 for TE₀, which means when the film is thinner than d_0 no TE mode can propagate in the film. The cut-off thickness is further discussed in Chap. 5.

Now we must take the corrugation into consideration. Instead of using mirrors, the DFB resonator provides optical feedback with a periodic corrugated microstructure. Coupled-wave theory can be used to explain how the microstructure couples free space light into and out of a waveguided mode [39, 40].

In a DFB laser, the grating leads to a periodic modulation of the effective refractive index of the optical mode propagating inside the active region. The index grating couples the forward and backward propagating waves through Bragg diffraction. Based on the coupled-wave theory, the intra-cavity electric field is written as

$$E(z) = (A(z) \exp(-ik_B z) + B(z) \exp(ik_B z)) \phi(x) \quad (2.19)$$

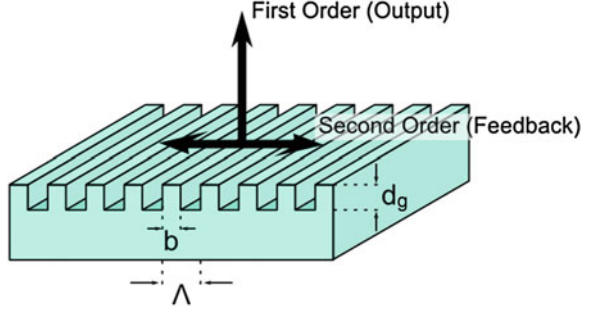
where $\phi(x)$ describes the guided wave, A and B are the amplitudes of the forward and backward propagating waves respectively and k_B is the Bragg wave-vector, defined by:

$$k_B = \frac{2\pi n_{eff}}{\lambda_B} = \frac{m\pi}{\Lambda} \quad (2.20)$$

where m is the diffraction order, n_{eff} is the effective refractive index experienced by the guided mode, λ_B is the Bragg wavelength and Λ is the grating period. Equation (2.20) is also known as the Bragg condition for in-plane feedback in a thin film waveguide. When $m = 1$, the feedback is provided by first order Bragg scattering in-plane. In this case, the laser beam is emitted from the edge of the film; it is so-called edge-emitting DFB lasers or first order DFB lasers. When $m = 2$, it is a second order laser, whose output coupling is normal to the film plane due to the first order diffraction, and optical feedback is provided by the in-plane second order Bragg scattering, as shown in Fig. 2.16.

$A(z)$ and $B(z)$ in Eq. (2.19) are solutions of the coupled-wave equation:

Fig. 2.16 First and second orders Bragg scattering in a surface emitting DFB laser



$$\left[\frac{\Delta\omega}{v_g} + i\left(\frac{\alpha - g}{2} + h_1\right) + i\frac{d}{dz} \right] A + (h_2 + ih_1)B = 0 \quad (2.21)$$

$$(h_2 + ih_1)A + \left[\frac{\Delta\omega}{v_g} + i\left(\frac{\alpha - g}{2} + h_1\right) - i\frac{d}{dz} \right] B = 0 \quad (2.22)$$

where h_1 is the coupling coefficient arising from two first-order diffractions and h_2 is the coupling coefficient arising from a second-order diffraction, while the other terms describe the complex changes in refractive index caused by angular frequency detuning $\Delta\omega$ from the Bragg frequency and net gain $g - \alpha$, and v_g is the group velocity [40]. In a second-order DFB laser, h_1 describes the radiation coupling loss while h_2 describes the feedback coupling coefficient. The values of h_1 and h_2 are given by

$$h_1 = \frac{\omega^4 \Delta\epsilon^2}{4k_0 k_x c^4} \left| \int dx \exp(ik_x x) \phi(x) \xi_1(x) \right|^2 \quad (2.23)$$

$$h_2 = -\frac{\omega^2 \Delta\epsilon}{2k_0 c^2} \int dx \phi(x)^2 \xi_2(x) \quad (2.24)$$

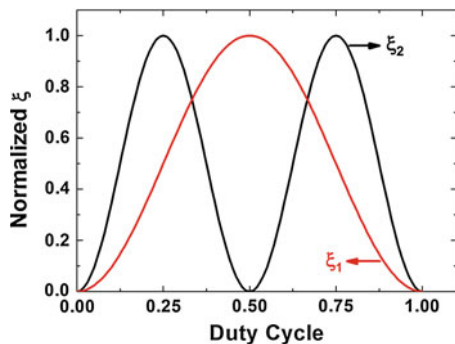
where $\exp(ik_x x)$ approximately describes the scattered wave in the x direction, $\Delta\epsilon$ is the dielectric change in the grating, ξ_1 and ξ_2 are the Fourier coefficients of the grating at position x . For a rectangular grating, ξ is defined by

$$\xi_m = \frac{\sin(m\pi b/\Lambda)}{m\pi} \quad (2.25)$$

where b is the width of the ridge of the grating, as shown in Fig. 2.16, b/Λ is known as the duty-cycle of the grating and m is an integer [41]. Normalized modulus of ξ_1 and ξ_2 are plotted against the duty-cycle in the range between 0 and 1 in Fig. 2.17. For a shallow grating, the relation between h_1 and h_2 can be expressed as:

$$\frac{h_1}{h_2} \cong \frac{\Delta\epsilon d_g}{n\lambda} \tan\left(\frac{\pi b}{\Lambda}\right) \quad (2.26)$$

Fig. 2.17 Normalized modulus of ξ_1 and ξ_2 as a function of the duty-cycle



where d_g is the groove depth. Experimental work has shown that for 50 % duty cycle, the first-order diffraction effectively built up stimulated emission in a first-order laser hence low threshold, while a duty cycle of 25 % gives the lowest lasing threshold by optimizing the in-plane feedback in second-order DFB lasers [42]. Varying the grating depth has also shown some influence on the organic laser threshold in Navarro-Fuster *et al*'s work [43, 44].

In Eq. (2.20), it is evident that the Bragg scattering angle is wavelength dependent. In Fig. 2.18, θ is the output coupling angle of the optical mode to the normal direction and φ is the in-plane propagation direction. The parameters k_x and k_y define two wave-vector components in the plane of the waveguide, perpendicular and parallel to the grating grooves. The magnitude of the in-plane wave-vector of the guided mode, k_{mode} , is coupled into a free-space wave at angle (θ, φ) by:

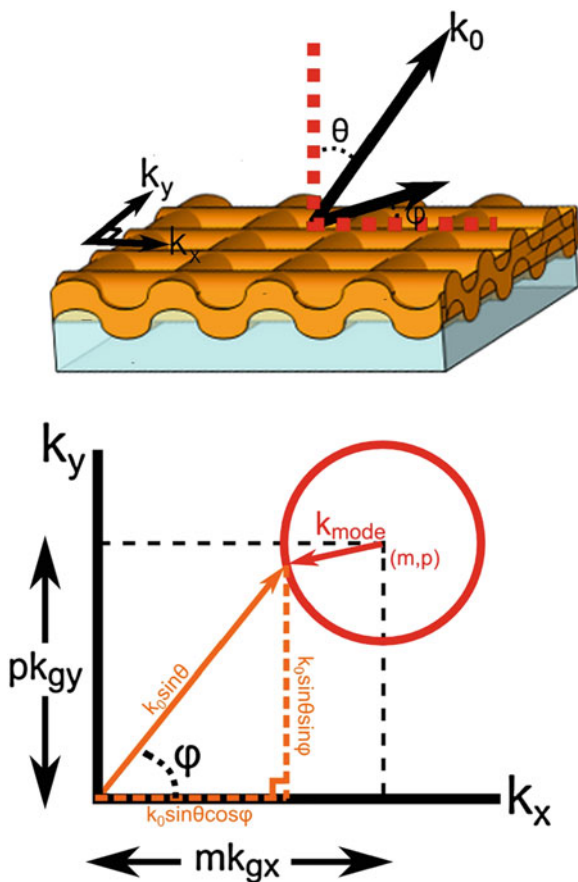
$$k_{mode}^2 = (mk_{gx} - k_0 \sin \theta \cos \varphi)^2 + (pk_{gy} - k_0 \sin \theta \sin \varphi)^2 \quad (2.27)$$

where k_{gx} and k_{gy} are the two orthogonal grating vectors, while m and p determine the order of the scattering process [45]. Equation (2.27) is illustrated diagrammatically in Fig. 2.18, where the magnitude of k_{mode} , i.e. the diameter of the mode circle, is given by $2\pi n_{eff}/\lambda$, and hence varies with the photon frequency. This can be experimentally observed by an angle-resolved photoluminescence measurement in one dimension (i.e. $\varphi = 0$). Equation (2.27) can be rewritten as

$$\pm \frac{2\pi n_{eff}}{\lambda} = m \frac{2\pi}{\Lambda} - \frac{2\pi}{\lambda} \sin \theta \quad (2.28)$$

Figure 2.19 shows an example of angle-dependent emission for $\varphi = 0$ [46]. In the left figure, the 'X' shaped pattern corresponds to the PL that emits into the guided transverse mode and is subsequently Bragg scattered out of the waveguide. A is a photonic stop-band where the propagation in the waveguide is forbidden; B and C are edges of the stop-band, where standing waves form in the thin film. In the right figure, lasing occurs at point B, i.e. on the long-wavelength edge of the stop band, where the largest gain is experienced. The stop-band is seen as a dip in

Fig. 2.18 (Top) light scattering in a corrugated film; (bottom) vector space for momentum conservation



the emission spectrum observed in the normal direction to the film below laser threshold. An example of an emission spectrum below and above laser threshold is shown in Fig. 2.20a, along with the shapes of output beams observed from a 1D and 2D second-order DFB lasers in far field. Lasing occurred only on the long-wavelength side of the stop-band because the output coupling loss of the standing wave field at the long-wavelength band edge is much lower than at the short-wavelength band edge, hence a lower lasing threshold for the long-wavelength mode [47]. The laser emission from 1D DFB resonators forms a ‘double-fan’ shaped pattern and is very divergent in the direction parallel to the orientation of the grating grooves due to the lack of optical confinement [48]. In the case of a 2D DFB laser, the emission pattern when the pump intensity is far above threshold is formed into a cross shape as a result of the 2D resonator, which is equivalent to two identical 1D gratings perpendicular to each other.

The out-coupled emission of the DFB laser represents a loss mechanism and thus increases the laser threshold. Therefore in theory the first-order DFB resonator

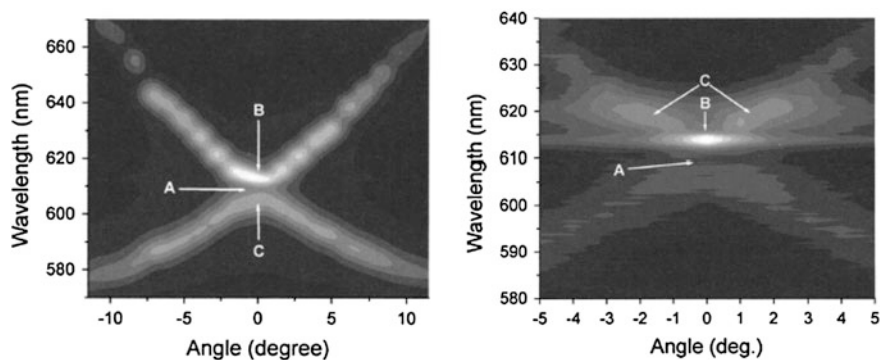
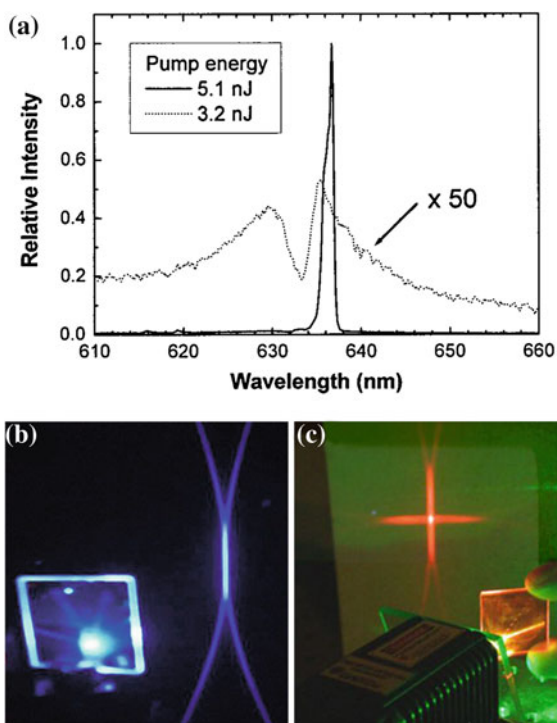


Fig. 2.19 Angle-dependent measurement for PL (*left*) and lasing (*right*) [46]. Reprinted with permission from Turnbull, G. A., Andrew, P., Jory, M. J., Barnes, W. L., Samuel, I. D. W. (2001) *Physical Review B*, 64, 125122. Copyright (2001) by the American Physical Society

Fig. 2.20 a Emission spectra detected in normal direction to a MEH-PPV waveguide plane, for pump energies below and above lasing threshold [47]; output beam observed respectively from **b** a 1-D PFO laser and **c** a 2-D MEH-PPV laser



is preferred in order to achieve lower threshold operation. However, lasers based on this type of grating emit from the edge of the resonator. Due to the fact that cleaved edges are not easy with amorphous organic layers, the creation of a well

defined edge for light emission is difficult. The output beam quality is also poor in this case.

In 2007, Karnutsch et al. reported a blue-emitting fluorene-based copolymer laser based on a mixed-order distributed feedback resonator - a second-order Bragg scattering region surrounded by first-order scattering regions [49]. The idea of the mixed-order resonator is that the second-order region provides some vertical outcoupling of the laser radiation while the first-order regions provide strong feedback. A very low laser threshold of 36 nJ/cm^2 (equivalent to 3.6 W/cm^2) was realized with this resonator. To date, this is the world-record for lowest organic semiconductor laser threshold. This special type of resonator is further discussed in Chap. 6.

2.5.2 Pump Sources for Organic Lasers

Compared to the simple fabrication and small size of inexpensive organic semiconductor lasers, the pumping source for organic semiconductor lasers becomes one of the major factors which complicates the design and increases the cost, which would limit the potential applications. Many different pump lasers have been used for pumping OSLs, such as dye lasers, nitrogen lasers, optical parametric oscillators (OPOs) and so on. By using a DFB resonator the laser threshold has been dramatically reduced, making pump light sources with lower output power feasible.

Microchip lasers with size about $10 \times 5 \times 5 \text{ cm}$ are commonly used in low threshold organic laser systems. More recently, polymer lasers pumped by a more compact and cheaper pump source, InGaN laser diode, have been demonstrated [50]. An InGaN laser diode emitting at 407 nm with maximum output energy about 0.67 nJ at 10 kHz repetition rate was used to pump DBR laser based on MEH-PPV blended with dye. The lasing threshold was as low as 0.42 nJ. Alternatively, blue-emitting lasers made of PFO doped with DPAVB were also pumped by InGaN diode lasers [51].

Since the first demonstration of an organic semiconductor laser, there has been great interest in making electrically pumped polymer lasers, however, it is extremely challenging mainly due to the following reasons [52]:

- High charge-carrier mobility in one gain material is essential in order to reduce the impact of singlet-triplet/polaron annihilations and induced absorption losses including polaron and triplet absorption. Charge-carrier mobilities of at least $5 \times 10^{-2} \text{ cm}^2/\text{Vs}$ are predicted to be required in order to achieve laser operation at a current density of about 10 kA/cm^2 [53], however, commonly used organic laser gain media have mobilities of only about $10^{-4} \text{ cm}^2/\text{Vs}$. Enhancement has been achieved, with β -phase PFO for example, the improved mobility can reach $8 \times 10^{-3} \text{ cm}^2/\text{Vs}$ [56];

- To pump above threshold, a current density of at least a few kA/cm^2 is required. However, the non-radiative losses such as singlet-polaron annihilation would increase with excitation strength at the same time;
- Significant losses are incurred at the metal contacts. From a study of the behaviour of Alq_3 with metal contacts, injection is seriously limited by electron trapping at the $\text{Alq}_3/\text{metal}$ interface [54];
- Thermal stability of organic semiconductors with such high density current injection is poor [55, 56].

In 2008, a big step to address this problem was the demonstration of first indirect electrically pumped polymer laser [57]. The integration of polymer lasers with high-power nitride LEDs provided a compact and convenient electrically controlled laser device. Compared to other laser pump sources for OSLs, the InGaN LEDs are electronically and physically more robust, and much cheaper. In the same year, an electrically driven hybrid light source in the visible wavelength range was demonstrated [58]. Thin conjugated polymer films were spin-coated on nano-structured DFB gratings which were combined directly upon an inorganic LED, as shown in Fig. 2.21. With this structure, electrically generated 390 nm ultraviolet light was transferred into an organic polymer layer via optical pumping and out-coupled green light by the second-order DFB grating, although only line-narrowed fluorescence was observed in this case. Indirect electrically pumped organic semiconductor lasers are discussed in Chaps. 5 and 6.

So far all organic semiconductor lasers are pumped under pulsed conditions rather than CW conditions. The reason for this is the excitons lifetime is short—between hundreds of picoseconds and a few nanoseconds and so required high excitation densities to maintain the population inversion. Non-radiative decays from intersystem crossing, excited-state absorption and exciton–exciton annihilation can dramatically increase the cavity losses and thus reduce the net gain. The ideal pulse duration of the pump source should be less than a nanosecond with a low repetition rate so that there is enough time for the long-lived excited states to relax before the next pulse arrives. For the field of organic semiconductor lasers,

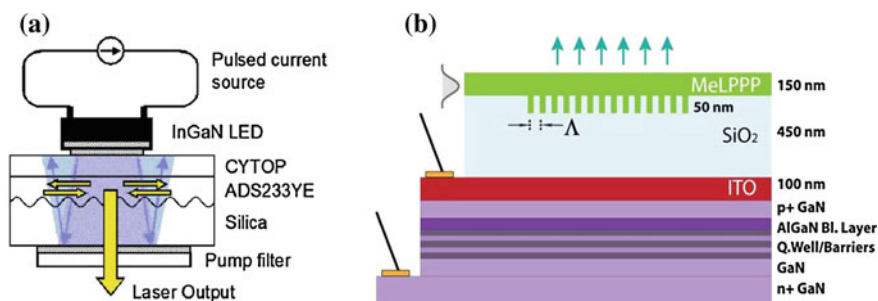


Fig. 2.21 **a** Hybrid InGaN LED pumped polymer laser; [57] **b** a compact light source that incorporates an inorganic LED, DFB grating and light-emitting polymer layer [58]

achieving CW/quasi-CW operation is an important challenge [59, 60]. The lasing thresholds with different pump pulse durations are studied in Chaps. 5 and 6.

References

1. Maiman, T. H. (1960). Optical and microwave-optical experiments in ruby. *Physical Review Letters*, 4(11), 546–566.
2. Hall, R. N., Fenner, G. E., Kingsley, J. D., Soltys, T. J., & Carlson, R. O. (1962). Coherent light emission from GaAs junctions. *Physical Review Letters*, 9(9), 366–368.
3. Nathan, M. I., Dumke, W. P., Burns, G., Dill, F. H., & Lasher, G. (1962). Stimulated emission of radiation from GaAs pn junctions. *Applied Physics Letters*, 1(3), 62–64.
4. Holonyak, Nick, & Bevacqua, S. F. (1962). Coherent (Visible) light emission from Ga(As_{1-x}P_x) junctions. *Applied Physics Letters*, 1(4), 82–83.
5. Alferov, Zh I, Andreev, V. M., Portno, E. L., & Trukan, M. K. (1969). *Sov. Phys. Semicond*, 3, 1107.
6. Hayashi, I., Panish, M. B., Foy, P. W., & Sumski, S. (1970). *Applied Physics Letters*, 17, 109.
7. Moses, D. (1992). High quantum efficiency luminescence from a conducting polymer in solution—a novel polymer laser-dye. *Applied Physics Letters*, 60(26), 3215–3216.
8. Tessler, N., Denton, G. J., & Friend, R. H. (1996). Lasing from conjugated-polymer microcavities. *Nature*, 382(6593), 695–697.
9. Clayden, J., Greeves, N., Warren, S. (2001). *Organic chemistry* (2nd ed.) Oxford: Oxford University Press.
10. Lewis, G. N., & Kasha, M. (1944). Phosphorescence and the triplet state. *Journal of the American Chemical Society*, 66(12), 2100–2116.
11. Kepler, R. G., Valencia, V. S., Jacobs, S. J., & McNamara, J. J. (1996). Exciton-exciton annihilation in poly(p-phenylenevinylene) films. *Synthetic Met*, 78(3), 227–230.
12. Frolov, S. V., Vardeny, Z. V., & Yoshino, K. (1998). Cooperative and stimulated emission in poly(p-phenylene-vinylene) thin films and solutions. *Physical Review B*, 57(15), 9141–9147.
13. DiazGarcia, M. A., Hide, F., Schwartz, B. J., Andersson, M. R., Pei, Q. B., & Heeger, A. J. (1997). Plastic lasers: Semiconducting polymers as a new class of solid-state laser materials. *Synthetic Met*, 84(1–3), 455–462.
14. Lawrence, J. R., Turnbull, G. A., Samuel, I. D. W., Richards, G. J., & Burn, P. L. (2004). Optical amplification in a first-generation dendritic organic semiconductor. *Optics Letters*, 29(8), 869–871.
15. Lawrence, J. R., Nandas, E. B., Richards, G. J., Burn, P. L., & Samuel, I. D. W. (2007). Effect of generation and soft lithography on semiconducting dendrimer lasers. *Advanced Materials*, 19(19), 3000–3003.
16. Johansson, N., Salbeck, J., Bauer, J., Weissortel, F., Brooms, P., Andersson, A., et al. (1998). Solid-state amplified spontaneous emission in some spiro-type molecules: A new concept for the design of solid-state lasing molecules. *Advanced Materials*, 10(14), 1136–1141.
17. Kanibolotsky, A. L., Perepichka, I. F., & Skabara, P. J. (2010). Star-shaped pi-conjugated oligomers and their applications in organic electronics and photonics. *Chemical Society Reviews*, 39(7), 2695–2728.
18. Ribierre, J. C., Tsiminis, G., Richardson, S., Turnbull, G. A., Samuel, I. D. W., Barcena, H. S., et al. (2007). Amplified spontaneous emission and lasing properties of bisfluorene-cored dendrimers. *Applied Physics Letters*, 91(8), 081108.
19. Samuel, I. D. W., & Turnbull, G. A. (2007). Organic semiconductor lasers. *Chemical Reviews*, 107(4), 1272–1295.
20. Hedley, G. J. (2010). *Ultrafast photophysics of iridium complexes*. Thesis for Doctor of Philosophy, University of St Andrews.

21. Frank, J. (1925). Elementary processes of photochemical reactions. *Transactions of the Faraday Society*, 21, 536–542.
22. Lakowicz, J. R. (1983). *Principles of fluorescence spectroscopy*. New York: Plenum Press.
23. Gupta, R., Stevenson, M., Dogariu, A., McGehee, M. D., Park, J. Y., Srdanov, V., et al. (1998). Low-threshold amplified spontaneous emission in blends of conjugated polymers. *Applied Physics Letters*, 73(24), 3492–3494.
24. Mattoussi, H., Murata, H., Merritt, C. D., Iizumi, Y., Kido, J., & Kafafi, Z. H. (1999). Photoluminescence quantum yield of pure and molecularly doped organic solid films. *Journal of Applied Physics*, 86(5), 2642–2650.
25. Pope, M., Swenberg, C. E. (1999). *Electronic processes in organic crystals and polymers* (2nd ed.). Oxford: Oxford University Press.
26. Kasha, M. (1947). Phosphorescence and the role of the triplet state in the electronic excitation of complex molecules. *Chemical Reviews*, 41(2), 401–419.
27. Baldo, M. A., O'Brien, D. F., You, Y., Shoustikov, A., Sibley, S., Thompson, M. E., et al. (1998). Highly efficient phosphorescent emission from organic electroluminescent devices. *Nature*, 395(6698), 151–154.
28. Kawamura, Y., Goushi, K., Brooks, J., Brown, J. J., Sasabe, H., & Adachi, C. (2005). 100% phosphorescence quantum efficiency of Ir(III) complexes in organic semiconductor films. *Applied Physics Letters*, 86(7), 071104.
29. Greenham, N. C., Samuel, I. D. W., Hayes, G. R., Phillips, R. T., Kessener, Y. A. R. R., Moratti, S. C., Holmes, A. B., Friend, R. H. (1995). Measurement of absolute photoluminescence quantum efficiencies in conjugated polymers. *Chemical Physics Letters* 241, 89–96.
30. Svelto, O., Hanna, D. C. (1998). *Principles of lasers* (4th ed.). New York: Springer.
31. Jenekhe, S. A., & Osaheni, J. A. (1994). Excimers and exciplexes of conjugated polymers. *Science*, 265(5173), 765–768.
32. Petrovic, J., Matavulj, P., Pinto, L., & Selmic, S. Z. (2009). Field induced singlet exciton dissociation and exciton–exciton Annihilation in MEH-PPV films studied by photocurrent spectra. *Acta Physica Polonica A*, 116(4), 595–597.
33. Shukla, A., Ghosh, H., & Mazumdar, S. (2004). Ultrafast excited state absorption and charge separation in phenylene-based conjugated polymers. *Synthetic Met*, 141(1–2), 59–65.
34. McBranch, D. W., Kraabel, B., Xu, S., Kohlman, R. S., Klimov, V. I., Bradley, D. D. C., et al. (1999). Signatures of excitons and polaron pairs in the femtosecond excited-state absorption spectra of phenylene-based conjugated polymers and oligomers. *Synthetic Met*, 101(1–3), 291–294.
35. McGehee, M. D., Gupta, R., Veenstra, S., Miller, E. K., Diaz-Garcia, M. A., & Heeger, A. J. (1998). Amplified spontaneous emission from photopumped films of a conjugated polymer. *Physical Review B*, 58(11), 7035–7039.
36. Tessler, N. (1999). Lasers based on semiconducting organic materials. *Advanced Materials*, 11(5), 363–370.
37. Chenais, S., & Forget, S. (2012). Recent advances in solid-state organic lasers. *Polymer International*, 61(3), 390–406.
38. Buckman, A. B. (1995). *Guided-wave photonics*. Oxford: Oxford University Press.
39. Moharam, M. G., Grann, E. B., Pommet, D. A., & Gaylord, T. K. (1995). Formulation for stable and efficient implementation of the rigorous coupled-wave analysis of binary gratings. *Journal of the Optical Society of America A: Optics, Image Science, and Vision*, 12(5), 1068–1076.
40. Kazarinov, R. F., Henry, C. H. (1985). Second-order distributed feedback lasers with mode selection provided by first-order radiation losses. *IEEE Journal of Quantum Electronics*, QE-21(2), 144–150.
41. Barlow, G. F., Shore, A., Turnbull, G. A., & Samuel, I. D. W. (2004). Design and analysis of a low-threshold polymer circular-grating distributed-feedback laser. *Journal of Optical Society of American B: Optical Physics*, 21(12), 2142–2150.

42. Turnbull, G. A., Carleton, A., Barlow, G. F., Tahraoui, A., Krauss, T. F., Shore, K. A., et al. (2005). Influence of grating characteristics on the operation of circular-grating distributed-feedback polymer lasers. *Journal of Applied Physics*, 98(2), 023105.
43. Kogelnik, H., & Shank, C. V. (1972). Coupled-wave theory of distributed feedback lasers. *Journal of Applied Physics*, 43(5), 2327–2335.
44. Navarro-Fuster, V., Vragovic, I., Calzado, E. M., Boj, P. G., Quintana, J. A., Villalvilla, J. M., et al. (2012). Film thickness and grating depth variation in organic second-order distributed feedback lasers. *Journal of Applied Physics*, 112, 043104.
45. Turnbull, G. A., Andrew, P., Barnes, W. L., & Samuel, I. D. W. (2003). Photonic mode dispersion of a two-dimensional distributed feedback polymer laser. *Physical Review B*, 67(16), 165107.
46. Turnbull, G. A., Andrew, P., Jory, M. J., Barnes, W. L., & Samuel, I. D. W. (2001). Relationship between photonic band structure and emission characteristics of a polymer distributed feedback laser. *Physical Review B*, 64(12), 125122.
47. Turnbull, G. A., Andrew, P., Barnes, W. L., & Samuel, I. D. W. (2003). Operating characteristics of a semiconducting polymer laser pumped by a microchip laser. *Applied Physics Letters*, 82(3), 313–315.
48. Heliotis, G., Xia, R. D., Turnbull, G. A., Andrew, P., Barnes, W. L., Samuel, I. D. W., et al. (2004). Emission characteristics and performance comparison of polyfluorene lasers with one- and two-dimensional distributed feedback. *Advanced Functional Materials*, 14(1), 91–97.
49. Karnutsch, C., Pflumm, C., Heliotis, G., Demello, J. C., Bradley, D. D. C., Wang, J., et al. (2007). Improved organic semiconductor lasers based on a mixed-order distributed feedback resonator design. *Applied Physics Letters*, 90(13), 131104.
50. Vasdekis, A. E., Tsiminis, G., Ribierre, J. C., O’Faolain, L., Krauss, T. F., Turnbull, G. A., et al. (2006). Diode pumped distributed Bragg reflector lasers based on a dye-to-polymer energy transfer blend. *Optics Express*, 14(20), 9211–9216.
51. Riedl, T., Rabe, T., Johannes, H. H., Kowalsky, W., Wang, J., Weimann, T., et al. (2006). Tunable organic thin-film laser pumped by an inorganic violet diode laser. *Applied Physics Letters*, 88(24), 241116.
52. Baldo, M. A., Holmes, R. J., & Forrest, S. R. (2002). Prospects for electrically pumped organic lasers. *Physical Review B*, 66(3), 035321.
53. Gärtner, C. (2008). Organic laser diodes—modelling and simulation. Thesis for Doctor of Philosophy, University of Karlsruhe.
54. Baldo, M. A., & Forrest, S. R. (2001). Interface-limited injection in amorphous organic semiconductors. *Physical Review B*, 64(8), 085201.
55. Kulkarni, A. P., Tonzola, C. J., Babel, A., & Jenekhe, S. A. (2004). Electron transport materials for organic light-emitting diodes. *Chemistry of Materials*, 16(23), 4556–4573.
56. Prins, P., Grozema, F. C., Nehls, B. S., Farrell, T., Scherf, U., & Siebbeles, L. D. A. (2006). Enhanced charge-carrier mobility in β -phase polyfluorene. *Physical Review B*, 74, 113203.
57. Yang, Y., Turnbull, G. A., & Samuel, I. D. W. (2008). Hybrid optoelectronics: A polymer laser pumped by a nitride light-emitting diode. *Applied Physics Letters*, 92(16), 163306.
58. Butun, B., Aydin, K., Ulker, E., Cheylan, S., Badenes, G., Forster, M., et al. (2008). A hybrid light source with integrated inorganic light-emitting diode and organic polymer distributed feedback grating. *Nanotechnology*, 19, 195202.
59. Giebink, N. C., & Forrest, S. R. (2009). Temporal response of optically pumped organic semiconductor lasers and its implication for reaching threshold under electrical excitation. *Physical Review B*, 79(7), 073302.
60. Zhang, Y. F., & Forrest, S. R. (2011). Existence of continuous-wave threshold for organic semiconductor lasers. *Physical Review B*, 84(24), 241301.

Low Threshold Organic Semiconductor Lasers
Hybrid Optoelectronics and Applications as Explosive
Sensors

Wang, Y.

2014, XVI, 164 p. 137 illus., 73 illus. in color., Hardcover

ISBN: 978-3-319-01266-7